arXiv:cond-mat/0209528v1 [cond-mat.soft] 23 Sep 2002

Free energy determination of phase coexistence in model C_{60}: A comprehensive Monte Carlo study

D. Costa*, G. Pellicane, M. C. Abramo, and C. Caccamo
Istituto Nazionale per la Fisica della Materia (INFM) and Dipartimento di Fisica
Università di Messina, Contrada Papardo, C.P. 50, 98166 Messina – Italy

The free energy of the solid and fluid phases of the Girifalco C_{60} model are determined through extensive Monte Carlo simulations. In this model the molecules interact through a spherical pair potential, characterized by a narrow and attractive well, adjacent to a harshly repulsive core. We have used the Widom test particle method and a mapping from an Einstein crystal, in order to estimate the absolute free energy in the fluid and solid phases, respectively; we have then determined the free energy along several isotherms, and the whole phase diagram, by means of standard thermodynamic integrations. The dependence of the simulation's results on the size of the sample is also monitored in a number of cases.

We highlight how the interplay between the liquid-vapor and the liquid-solid coexistence conditions determines the existence of a narrow liquid pocket in the phase diagram, whose stability is assessed and confirmed in agreement with previous studies. In particular, the critical temperature follows closely an extended corresponding-states rule recently outlined by Noro and Frenkel [J. Chem. Phys. **113**, 2941 (2000)].

We discuss the emerging "energetic" properties of the system, which drive the phase behavior in systems interacting through short-range forces [A. A. Louis, Phil. Trans. R. Soc. A **359**, 939 (2001)], in order to explain the discrepancy between the predictions of several structural indicators and the results of full free energy calculations, to locate the fluid phase boundaries.

More generally, we aim to provide extended reference data for calculations of the free energy of the C_{60} fullerite in the low temperature regime, as for the determination of the phase diagram of higher order $C_{n>60}$ fullerenes and other fullerene-related materials, whose description is based on the same model adopted in this work.

PACS numbers: 61.48.+c, 64.70.Fx

I. INTRODUCTION

We report an extensive investigation of the free energy characteristics of the Girifalco model of C_{60} fullerene [1]. As is well known, this representation hinges on the fact that C_{60} molecules have almost spherical shape and freely rotate at sufficiently high temperatures [2]. Under these conditions, the hollow molecular cages can be assimilated to spheres whose surface consists of a uniform distribution of carbon sites. The overall interaction between two fullerene particles is then obtained by an integral of the interaction between pairs of sites on different cages, eventually yielding an analytic central two-body potential. The latter is characterized by a harshly repulsive core at short distance, followed by a deep attractive well which rapidly decays with the interparticle distance [1].

The Girifalco model constitutes a prototype system in several respects; recent studies suggest that a similar "smeared out" spherical description can be attempted for $C_{n>60}$ systems, although fullerene molecules with $n > 60$ can have a sensibly non-spherical shape; the cases $n = 70$, 76 and 84 have in particular been examined (see [3] and references therein). On the other hand, more refined calculations of the fullerene-fullerene interaction yield results very close to those predicted through the Girifalco model [4,5], and a similar representation has been used for the description of other hollow nanoparticles as carbon onions, or metal dichalcogenides (also termed inorganic fullerenes) as GaAs and CdSe [6]. Moreover, a modification of the Girifalco model, suitable for the description of solid C_{60} at low temperatures, has been recently proposed [7]; this development seems of particular interest since fullerites, doped with organic molecules and upon the injection of electron (or holes), exhibit a superconducting behavior up to $T = 112$ K [8]; an accurate description of such a simple model might prove useful for further studies on the lattice behavior upon impurity doping.

In our opinion, such a possible reference role of the Girifalco model for further studies on fullerenes and other systems, calls for a complete and confident determination of its phase diagram. With this purpose in mind, we have investigated the free energy characteristics of the C_{60} model for both the solid and the fluid phase through

*Corresponding author, e-mail: costa@tritone.unime.it

extensive Monte Carlo simulations, spanning the whole high-temperature region of the phase diagram.

A second general aspect of the Girifalco potential is related to its short-range nature. It is useful to recall in this respect that a ubiquitous definition of the range of interaction has been recently proposed in Ref. [9]. As several studies have pointed out, the most apparent consequence of a reduced interaction length is the metastability of the liquid-vapor equilibrium, which is preempted by the fluid-solid coexistence [10]. It is actually known that a stable liquid-vapor coexistence still survives for the model envisaged here, albeit restricted to a few tens degree temperature range [11,12]. A tiny liquid pocket has been predicted also in the phase diagram of similar models of higher order fullerenes [3], although it is argued that even a modest reduction of the range of the forces might cause the disappearance of the liquid phase. The emerging borderline nature of the Girifalco model implies that the overall appearance of its phase diagram sensitively depends on the details of the interaction potential; in fact, the initial controversy around the existence of a stable liquid phase for this system [11,13] has been solved by taking into account on one side the full role of the attractive part of the interaction [14], and on the other, a conveniently large simulation sample [15]. More generally, it has been recognized in Ref. [16] that the physical behavior of a wide class of systems characterized by short-range interactions, and in particular the onset of freezing, are substantially affected by the "perturbative" part (with respect to the repulsive core) of the potential, rather than being dominated by excluded-volume and packing (i.e. by entropic) effects, as is the case in the currently accepted *van der Waals picture* of simple liquids [17]. We here investigate, as a further key purpose of this work, the same issue for the C_{60} model and try to reconcile the predictions coming from different structural indicators — usually related to the freezing threshold of several simple liquids [18,19] and adopted in early calculations for this model [11,20,21] — with the results of full free energy calculations.

The paper is organized as follows: we present in Section II the model and the simulation strategies; the results are reported and discussed in Sect. III, while Sect. IV is devoted to the conclusions and future perspectives of our investigation. A preliminary account of this work has been presented elsewhere [22].

II. MODEL AND SIMULATION STRATEGIES

The Girifalco potential between two C_{60} molecules, is written as [1]:

$$v(r) = -\alpha_1 \left[\frac{1}{s(s-1)^3} + \frac{1}{s(s+1)^3} - \frac{2}{s^4} \right] + \alpha_2 \left[\frac{1}{s(s-1)^9} + \frac{1}{s(s+1)^9} - \frac{2}{s^{10}} \right], \qquad (1)$$

where $s = r/d$, $\alpha_1 = N^2 A/12d^6$, and $\alpha_2 = N^2 B/90d^{12}$; $N = 60$ and $d = 0.71$ nm are the number of carbon atoms and the diameter, respectively, of the spherical particles; $A = 32 \times 10^{-60}$ erg cm^6 and $B = 55.77 \times 10^{-105}$ erg cm^{12} are constants entering the Lennard-Jones 12-6 potential through which two carbon sites on different molecules are assumed to interact. The finite distance at which the potential (1) crosses zero and the minimum of the potential well depth are $\sigma \simeq 0.959$ nm and $\varepsilon \simeq 0.444 \times 10^{-12}$ erg at $r_{\min} = 1.005$ nm, respectively.

In order to investigate the coexistence properties of model (1), it is required the knowledge of the free energies of both the solid and the fluid phase. As a general strategy, the free energy of the system is first evaluated all along a supercritical isotherm at temperature $\overline{T}$ by integrating the pressure P as a function of the density ρ according to the formula [23]:

$$\frac{\beta F(\rho,\overline{T})}{N} = \frac{\beta F(\overline{\rho},\overline{T})}{N} + \int_{\overline{\rho}}^{\rho} \frac{\beta P(\rho')}{\rho'} \frac{\mathrm{d}\rho'}{\rho'}\,; \qquad (2)$$

here F/N is the Helmholtz free energy per particle, $\beta = 1/k_B T$ is the inverse temperature, k_B is the Boltzmann constant and $(\overline{\rho},\overline{T})$ is a thermodynamic state where the free energy is known (see below). The free energy at different temperatures is then calculated along isochoric paths as:

$$\frac{\beta F(\rho,T)}{N} = \frac{\beta F(\rho,\overline{T})}{N} - \int_{\overline{T}}^{T} \frac{U(T')}{N k_B T'} \frac{\mathrm{d}T'}{T'}\,, \qquad (3)$$

where U/N is the internal energy per particle of the system. The equilibrium conditions finally derive from the equality of the chemical potential and the pressure of the different phases.

All quantities entering Eqs. (2) and (3) have been determined through standard Monte Carlo simulations at constant volume or pressure. Simulations have been mostly carried out on a sample composed of $N = 864$ C_{60} particles enclosed in a cubic box with periodic boundary conditions. The C_{60} interaction has been considered up to half the box length.

As far as the determination of the reference free energy $F(\overline{\rho},\overline{T})$ in Eq. (2) is concerned, we have used for the solid phase the Einstein crystal method described by Frenkel and Ladd [24,25]. Namely, the C_{60} interaction in the solid fullerite is smoothly transformed, through a coupling parameter λ, into a corresponding harmonic potential so that the configurational energy $U(\{\mathbf{r}\})$ takes the following form [25]:

$$U(\{\mathbf{r}\}) = U_{C_{60}}(\{\mathbf{r}_0\}) + (1-\lambda)\left[U_{C_{60}}(\{\mathbf{r}\}) - U_{C_{60}}(\{\mathbf{r}_0\})\right] + \lambda \sum_{i=1}^{N} \alpha (\mathbf{r}_i - \mathbf{r}_{0,i})^2\,, \qquad (4)$$

where $\mathbf{r}_{0,i}$ is the lattice position of atom i and $U_{C_{60}}(\{\mathbf{r}_0\})$ is the static contribution to the potential energy; α is the

spring constant of the Einstein crystal. The free energy difference can then be written as:

$$\frac{\beta F(\overline{\rho},\overline{T})}{N} \equiv \frac{\beta F_{\rm C_{60}}}{N} = \frac{\beta F_{\rm ein}}{N} + \int_1^0 {\rm d}\lambda \left\langle \frac{\beta}{N}\frac{\partial U(\lambda)}{\partial \lambda}\right\rangle_\lambda , \qquad (5)$$

where the configurational free energy of the Einstein crystal is:

$$\frac{\beta F_{\rm ein}}{N} = \frac{\beta U_{\rm C_{60}}(\{\mathbf{r}_0\})}{N} - \frac{3(N-1)}{2N}\ln\left(\frac{\pi}{\alpha\beta}\right) + \frac{3}{2N}\ln N - \frac{\ln V}{N} . \qquad (6)$$

In the equation above, the last two terms account for the fixed center of mass constraint at which simulations are performed [25].

As for the absolute free energy of the fluid phase, the chemical potential μ has been estimated at several intermediate densities through the Widom test particle method [25,26].

In parallel with the free energy, the entropy of the fluid phase is also systematically analyzed, given that in several earlier papers the onset of freezing of the Girifalco model has been associated with the vanishing of the *residual multiparticle entropy* Δs, namely

$$\Delta s \equiv s_{\rm ex} - s_2 = 0 , \qquad (7)$$

according to the one-phase freezing criterion originally proposed in Ref. [19]. In Eq. (7), $s_{\rm ex}$ is the the excess entropy per particle of the system (in k_B units) and s_2 is defined in terms of the radial distribution function $g(r)$ of the system as [27]:

$$s_2 = -\frac{\rho}{2}\int \{g(r)\ln[g(r)] - g(r) + 1\}\,{\rm d}\mathbf{r} . \qquad (8)$$

In previous works Δs has been evaluated using liquid state integral equation theories. Here we report Monte Carlo data for the structural and thermodynamics quantities entering Eqs. (7) and (8), in order to perform a rigorous test of the theoretical predictions based on the criterion (7).

III. RESULTS AND DISCUSSION

The solid and liquid branches of the equation of state, to be integrated in Eq. (2), have been calculated at the supercritical isotherm $\overline{T} = 2100$ K through both NVT and NPT Monte Carlo simulations, in order to cross-check the predictions of the two algorithms. Five to six runs of 25 000 steps have been performed at each thermodynamic point investigated. The compressibility factor $\beta P/\rho$ is shown in Fig 1.

Results for the absolute free energy of the solid phase at $\overline{T} = 2100$ K and $\overline{\rho} = 1.375$ nm^{-3}, as obtained through the Einstein crystal method, are reported in Fig. 2. Constant volume simulations have been carried out for several values of the switching parameter λ. The spring constant is set to a value $\alpha/\varepsilon = 490$, which makes the interactions in the pure Einstein crystal as close as possible to those of the original system, so to optmize the accuracy of the numerical integration scheme of Eq. (5) [25]. We have analyzed the free energy dependence on the system size; results with 256 and 2916 particles are shown in Fig. 2. It appears that the effect of N on the estimate of the free energy is small but systematic; in the thermodynamic limit ($N \to \infty$) the smooth extrapolation in the bottom panel of Fig. 2 yields $\beta F/N(\overline{\rho} = 1.375$ nm$^{-3}, \overline{T} = 2100$ K$) \simeq -1.401$.

As for the fluid phase, the excess chemical potential at $\overline{T} = 2100$ K and $\overline{\rho} = 0.60$ nm^{-3} has been calculated through the Widom test particle method as $\beta\mu_{\rm ex} = -1.523$. Several tests at higher densities have also been conducted, in order to assess the results obtained via Eq. (2). The free energy at $T = 2100$ K is shown in the top panel of Fig. 3, along with the common tangent construction, which determines the coexistence conditions. The μ *vs* P behavior is displayed in the bottom panel of Fig. 3; it emerges that the thermodynamic integration of Eq. (2) fully agrees with the direct estimate of the chemical potential based on the Widom technique.

Starting from the knowledge of the free energy along the isotherm $\overline{T} = 2100$ K, the free energy at different temperatures has been obtained through Eq. (3). We have examined the isochores $\rho = 1.25$, 1.27, and 1.30 nm^{-3} in the solid phase and the density range $\rho = [0.70 - 1.00]$ nm^{-3} with steps $\Delta\rho = 0.05$ nm^{-3} in the liquid phase, descending down to $T = 1800$ K, with temperature intervals $\Delta T = 25$ K. Simulations have been carried out with $N = 864$ particles at constant density; four to eight cumulation runs of 10 000 steps at each state point are sufficient to yield accurate internal energies estimates (see Fig. 4), so to allow a smooth interpolation for the integration in Eq. (3). The pressure and the free energy along several isotherms are shown in Figs. 5 and 6, respectively; fully consistent results are obtained if we determine the free energy along an isochoric path first, and then integrating Eq. (2) at constant temperature. The accuracy of this global check is also evidenced in Fig. 6.

In order to analyze the thermodynamic properties of the system in the low density regime $\rho = [0.05 - 0.20]$ nm^{-3}, we have calculated the chemical potential of the vapor phase along the isotherm $T = 1900$ K through the Widom technique, and then estimated through Eq. (3) the free energy in the temperature range $T = [1800 - 1900]$ K.

As is visible in Fig. 7, where the chemical potential of the different phases is shown, liquid-solid equilibrium is stable at $T = 1900$, while a solid-vapor coexistence takes place at $T = 1850$ K. The intermediate temperature $T = 1875$ K is characterized by almost a compara-

ble value of the chemical potential of the various phases. We thus estimate that the triple point temperature is $T_{\rm tr} \simeq 1875$ K, at the pressure $P_{\rm tr} \simeq 2.4$ MPa; we then obtain from the equation of state $\rho_{\rm tr} \simeq 0.74$ nm^{-3}, in close agreement with the free energy results of Ref. [12], $T = 1880$ K and $\rho = 0.74$ nm^{-3}. The features in the μ *vs* P behavior which determine the narrow temperature width of the liquid pocket are clearly illustrated in Fig. 7, where it emerges that the solid and the liquid free energy branches have dissimilar slopes and considerably different spacing under equal variations of temperature. These two circumstances cause a fairly rapid shift of the liquid-solid intersection points and hence of the corresponding equilibrium parameters. Conversely, the vapor branch is hardly sensitive to temperature variations, and already at $T \gtrsim 1900$ K tends to loose any further intersection with both the solid and the liquid branch. The only surviving liquid-solid equilibrium therefore fully characterizes the system behavior for $T > 1950$ K.

The phase diagram of the system is displayed in Fig. 8, along with our previous Gibbs Ensemble Monte Carlo (GEMC) determination of the binodal line [15]. Distinct liquid-vapor and liquid-solid equilibria take place at temperatures slightly higher than 1875 K; as far as the liquid-vapor coexistence is concerned, we observe a remarkable agreement between free energy calculations and GEMC results. At lower temperatures, the binodal points are metastable with respect to the freezing line; in this case as well, the GEMC approach fully reproduce the free energy data. We thus retain the GEMC results $T_{\rm cr} \simeq 1940$ K, $\rho_{\rm cr} \simeq 0.42$ nm^{-3}, and $P_{\rm cr} \simeq 2.7$ MPa, obtained in Ref. [15] with 1500 C_{60} particles, as a reliable estimate of the critical point parameters. We note in this context that an extended correponding-state behavior, which states a linear relationship between the critical temperature and the range R of the interaction potential, has been recently outlined in Ref. [9]. R is defined by a map of the potential into an effective square well interaction with the same second virial coefficient. We obtain for the C_{60} model $R = 0.16$, a value immediately over the minimum threshold of a stable liquid-vapor equilibrium, $R = 0.13 - 0.15$ [9]; the extended rule's estimate for the critical temperature is then $T = 1922$ K, in fair agreement with the above $T_{\rm cr} = 1940$ K result.

A comparison with the phase diagram determined by Hagen and coworkers [13] is reported in Fig 8. It has been conjectured, on the basis of a theoretical density-functional investigation [14], that the emerging discrepancy between Ref. [13] results and subsequent calculations might be due to an early cutoff of the C_{60} interactions, which substantially affects the location of the liquid-vapor binodal line. We argued on the other hand [15], that a fairly large simulation sample should be employed in this case, in order to take into account the peculiar density fluctuations in the GEMC simulations, which act to destabilize the liquid-vapor separation. We note that, while the overall fluid phase boundaries can sensitively depend on the interaction details (and hence on the cutoff), truncation effects play a minor role in the determination of the melting line; the latter appears indeed coincident with our estimate, and almost independent on temperature variations, ranging from $\rho = 1.26$ nm^{-3} at $T = 2200$ K to $\rho = 1.28$ nm^{-3} at $T = 1800$ K. Our results positively agree with the phase diagram obtained in Ref. [12] (also shown in Fig. 8), where a slightly higher critical temperature $T = 1954 - 1980$ K is reported.

The phase diagram in the $P - T$ representation is displayed in Fig. 9, where it appears that also the pressure range of the liquid phase is rather restricted, spanning only a few tens bar over the triple point pressure $P_{\rm tr} = 2.4$ MPa.

We now turn to the indications on the freezing conditions obtained through the one-phase criterion expressed by Eq. (7). As is visible in Fig. 8, the $\Delta s = 0$ *locus* tends to overestimate the coexisting fluid density, thus affecting the location of the triple point in the phase diagram. We remark that a similar trend would emerge if the Hansen-Verlet prescription [18,23] for the height of the first peak of the structure factor were used [3]. In fact, the close correspondence between the two interpretations of the freezing transition in terms of structural indicators, has been recently pointed out in Ref. [28]. Similarly, the behavior of the internal energy, as well as the height of the first peak of the radial distribution function, show a non-monotonic behavior [21], suggesting that the system becomes unstable against the phase separation around the density $\rho \simeq 1.0$ nm^{-3} (see also Ref. [29]).

It thus appears that such indicators identify a very restricted range (if not a unique *locus*) of density *vs* temperature states, over which a structural reorganization of the fluid phase should be tendentially established, in order to satisfy purely excluded-volume, or equivalently entropic, demands. The almost vertical disposition of the $\Delta s = 0$ line (see Fig. 8), which means that the density keeps constant along the *locus* irrespective of the temperature, clearly reflects the substantial absence of any energy scale associated with such an indication. It is known at present that the vanishing of the residual multiparticle entropy accurately predicts the thermodynamic freezing threshold for a wide class of simple fluids, including hard-core models and the Lennard-Jones potential, in both three and two dimensions [28]. In these models, the interparticle potential is dominated by steric effects, while the attractive forces can be treated as a perturbation to the inherent hard-sphere system, which essentially drives the liquid behavior, an approach commonly called the *van der Waals picture* of fluids [17]. This is furthermore illustrated in Fig. 8, where it emerges that the reference hard-sphere system for the C_{60} model, obtained by splitting the potential into a repulsive and a perturbative part in the WCA fashion (after Weeks *et al* [30]), also freezes around the *locus* of vanishing residual multiparticle entropy, $\rho(T) \simeq 1.0$ nm^{-3}.

We argue that the discrepancy between one-phase indicators and full free energy calculations about the freezing

transition of the system at issue, leads to a different scenario, where the strong attractive and rapidly decaying well in the interaction potential critically affects the conditions for the onset of the solid-liquid transition. The latter is driven in this case by "energetic" rather than by entropic effects, in agreement with several indications recently collected for systems with short-range interactions by A. A. Louis [16]. It is shown in Ref. [16] that for this class of fluids most of the features exhibited by hard-sphere dominated systems do not arise, resulting in particular in the anticipation of the frezing threshold to lower densities than those predicted by solely structural conditions. In this respect, the lack of an accurate estimate of the freezing line of model C_{60} upon use of either the residual multiparticle entropy or the Hansen-Verlet prescriptions, must be interpreted less a "failure" of the criteria themselves, than a manifestation of their limited applicability in the present context, both indicators predicting the freezing threshold of the fluid on the basis of almost purely entropic requirements.

It appears in conclusion that the phase behavior of the Girifalco C_{60} model can be consistently understood in terms of general properties of systems interacting through short-range forces. Nevertheless, several issues are still open to further investigations and we refer firstly to the physical meaning to be associated to the fluid phase boundaries signalled by the above structural indicators. We note, on the other hand, the lack of clear indications of the freezing transition at a thermodynamic level, both in the internal energy and in the pressure, as documented in Figs. 4 and 5. More generally, the question of a detailed description of the microscopic behavior of the C_{60} model — as of other fluids interacting through short-range forces — already raised in Ref [31], is still unsolved. The formation of metastable clusters of strongly correlated particles in such fluids has been discussed in some recent papers [32], on the basis of the short-range nature of the interaction potential; however, in a recent molecular dynamics study [33] of quite a similar model, we have not been able to identify any net precursor, at a microscopic level, either of the fluid-solid threshold, or of the incipient crystallization of the liquid phase.

IV. CONCLUSIONS AND PERSPECTIVES

The free energy of the solid, liquid and vapor phases of the Girifalco model of C_{60} has been studied by means of extensive Monte Carlo simulations at constant density or pressure; the full phase diagram of the system has then been reconstructed on such a basis. It is confirmed by this comprehensive investigation that a stable liquid phase for this system exists, albeit confined to a rather restricted temperature range: we confidently estimate the triple and critical temperatures as $T_{\rm tr} \simeq 1875$ K and $T_{\rm cr} = 1940$ K, respectively. The pressure range of the liquid phase also appears rather narrow, spanning only a few tens bar over the triple point pressure. Our results illustrate how the interplay of various free energy branches determines the overall appearance of the phase diagram, and in particular the narrow extension of the liquid pocket.

The estimate of the freezing conditions, based on several structural indicators, is also critically discussed. It turns out that such indicators identify a practically unique thermodynamic *locus*, where the fluid phase becomes unfavoured due to entropic requirements. This *locus* almost coincides with the true thermodynamic freezing line for systems whose phase behavior is dominated by steric effects. For the model at issue, the solid-liquid transition is instead strongly affected by the deep, short-range attractive well in the interaction potential. As a result, the freezing transition of the fluid is driven to lower densities, mainly by energetic effects, in agreement with a scenario recently proposed by other authors.

As far as further studies are concerned, we are currently assessing, against the wide set of data produced in this work, the performances of several refined integral equation theories of the liquid state [34] and perturbation approaches, in order to describe on a full theoretical ground the phase diagram and the free energy properties of the Girifalco model. A refinement of our preliminary report on the phase diagram of higher order fullerenes $C_{n>60}$ [3] is also in progress. Finally, we plan to investigate the C_{60} properties, as well as the phase behavior of systems constituted by doped fullerites, in the low-temperature region of the solid phase.

[1] L. F. Girifalco, J. Phys. Chem. **95**, 5370 (1991); **96**, 858 (1992).

[2] C. M. Lieber and C.-C. Chen, *Solid State Physics* **48**, 109, H. Ehrenreich and F. Spaepen eds. (Academic Press, San Diego, 1994).

[3] M. C. Abramo, C. Caccamo, D. Costa, and G. Pellicane, Europhys. Lett. **54**, 468 (2001).

[4] J. Q. Broughton, J. V. Lill, and J. K. Johnson, Phys. Rev. B **55**, 2808 (1997).

[5] J. M. Pacheco and J. P. Prates-Ramalho, Phys. Rev. Lett. **79**, 3873 (1997); A. L. C. Ferreira, J. M. Pacheco and J. P. Prates-Ramalho, J. Chem. Phys. **113**, 738 (2000).

[6] U. S. Schwarz and S. A. Safran, Phys. Rev. E **62**, 6957 (2000).

[7] O. Umiguchi, T. Inaoka, and M. Hasegawa, J. Phys. Soc. Japan **68**, 508 (1999).

[8] J. H. Schon, C. Kloc, and B. Batlogg, Science **293**, 2432 (2001).

[9] M. G. Noro and D. Frenkel, J. Chem. Phys. **113**, 2941 (2000).

[10] M. H. J. Hagen and D. Frenkel, J. Chem. Phys. **101**, 4093 (1994); C. F. Tejero, A. Daanoun, H. N. W. Lekkerkerker,

and M. Baus, Phys. Rev. Lett. **73**, 752 (1994).
[11] A. Cheng, M. L. Klein, and C. Caccamo, Phys. Rev. Lett. **71**, 1200 (1993).
[12] M. Hasegawa and K. Ohno, J. Chem. Phys. **111**, 5955 (1999).
[13] M. H. J. Hagen, E. J. Meijer, G. C. A. M. Mooij, D. Frenkel, and H. N. W. Lekkerkerker Nature **365**, 425 (1993).
[14] M. Hasegawa and K. Ohno, J. Phys.: Cond. Matter **9**, 3361 (1997).
[15] C. Caccamo, D. Costa, and A. Fucile, J. Chem Phys. **106**, 255 (1997).
[16] A. A. Louis, Philos. T. Roy. Soc. A **359**, 939 (2001).
[17] D. Chandler, J. D. Weeks, and H. C. Andersen, Science **220**, 787 (1983).
[18] J.-P. Hansen and L. Verlet, Phys. Rev. **184**, 151 (1969).
[19] P. V. Giaquinta and G. Giunta, Physica A **187**, 145 (1992).
[20] C. Caccamo, Phys. Rev. B **51**, 3387 (1995).
[21] M. C. Abramo and G. Coppolino, Phys. Rev. B **58**, 2372 (1998).
[22] D. Costa, C. Caccamo, and M. C. Abramo, J. Phys.: Cond. Matter **14**, 2181 (2002).
[23] J.-P. Hansen and I. R. McDonald, *Theory of Simple Liquids* 2nd ed. (Academic Press, New York, 1986).
[24] D. Frenkel and A. J. C. Ladd, J. Chem. Phys. **81**, 3188 (1984).
[25] D. Frenkel and B. Smit, *Understanding Molecular Simulation* (Academic Press, London, 1996).
[26] B. Widom, J. Chem. Phys. **39**, 2808 (1963).
[27] R. E. Nettleton and M. S. Green, J. Chem. Phys. **29**, 1365 (1958).
[28] F. Saija, S. Prestipino, and P. V. Giaquinta, J. Chem. Phys. **113**, 2806 (2000); **115**, 7586 (2001), and references therein.
[29] M. Hasegawa and K. Ohno, J. Chem. Phys. **113**, 4315 (2000).
[30] J. D. Weeks, D. Chandler, and H. C. Andersen, J. Chem. Phys. **54**, 5237 (1971).
[31] N. W. Ashcroft, Nature **365**, 387 (1993).
[32] G. Foffi *et al*, Phys. Rev. E **65**, 031407 (2002); D. Pini, J. L. Ge, A. Parola, and L. Reatto, Chem. Phys. Lett. **327**, 209 (2000).
[33] D. Costa, P. Ballone, and C. Caccamo, J. Chem. Phys. **116**, 3327 (2002).
[34] C. Caccamo and G. Pellicane, *to appear in* J. Chem. Phys. (2002).

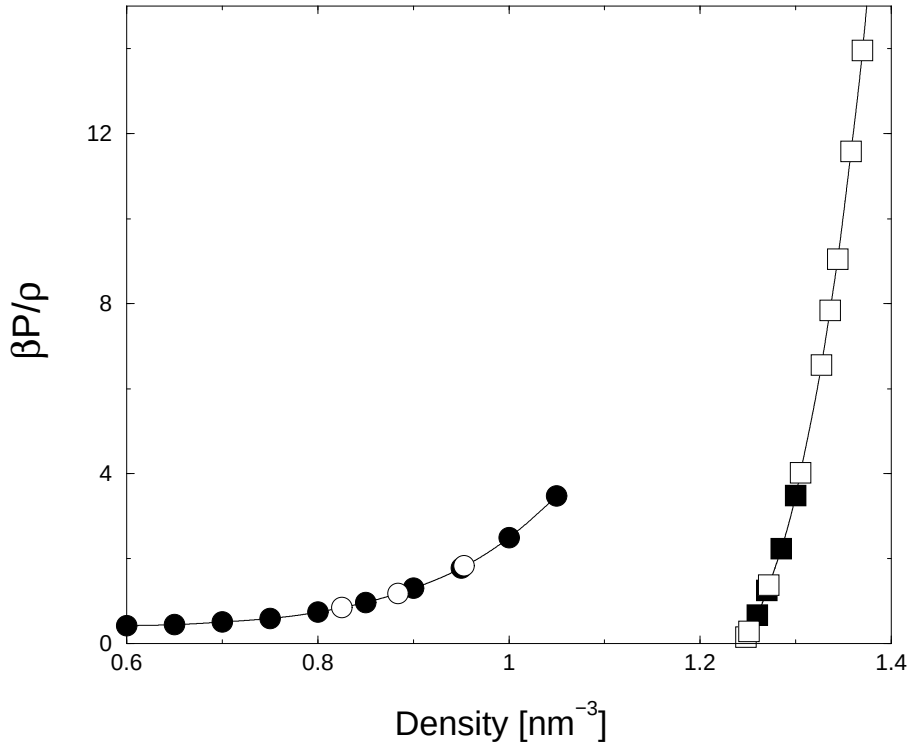


FIG. 1. Equation of state of the Girifalco model in the fluid (circles) and solid (squares) phases at $T = 2100$ K, as obtained through NVT (solid symbols) and NPT (open symbols) Monte Carlo simulations.

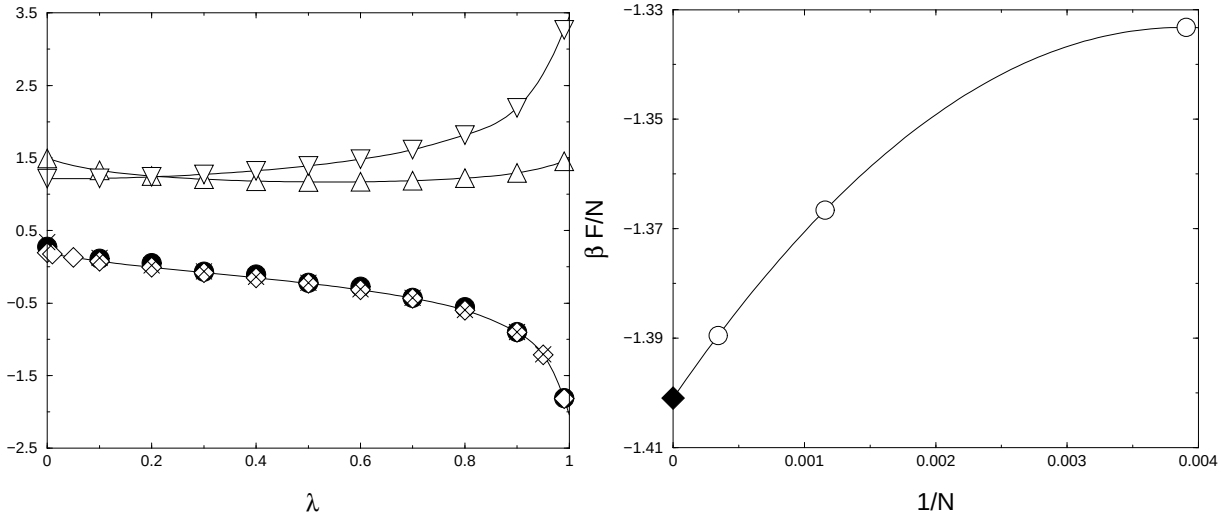


FIG. 2. Results of the Einstein crystal procedure for the determination of the free energy in the solid phase at $T = 2100$ K and $\rho = 1.375$ nm^{-3}. Left: integrand in Eq. (5) (circles), resolved into the harmonic (downward triangles) and C_{60} (upward triangles) contributions, see Eq. (4). Simulation results obtained with $N = 256$ (diamonds) and $N = 2916$ (crosses) particles are also shown. Lines are smooth interpolations of the data points. Right: size dependence of the free energy of the C_{60} crystal; the diamond indicates the extrapolation (solid line) to the thermodynamic limit.

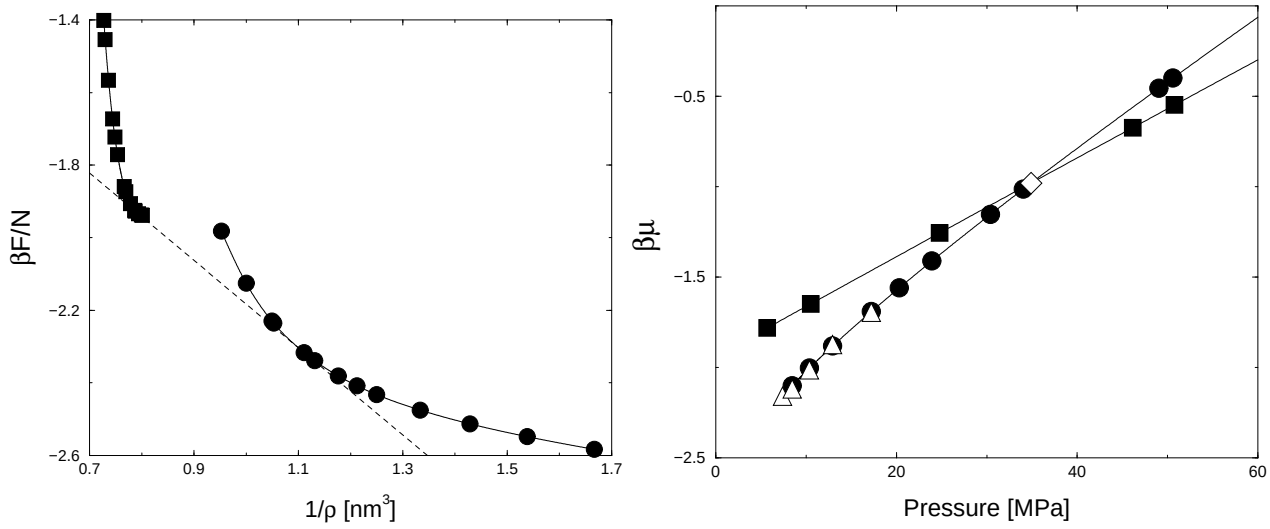


FIG. 3. Free energy (left) and chemical potential (right) of the C_{60} model along the isotherm $T = 2100$ K. Squares: solid phase; circles: fluid phase. Solid lines are smooth interpolations of the data points. In the left panel the common tangent construction (dashed line) is shown. In the right panel the diamond locates the coexistence conditions; the direct estimates of the chemical potential (triangles), based on the Widom test particle method, are also reported.

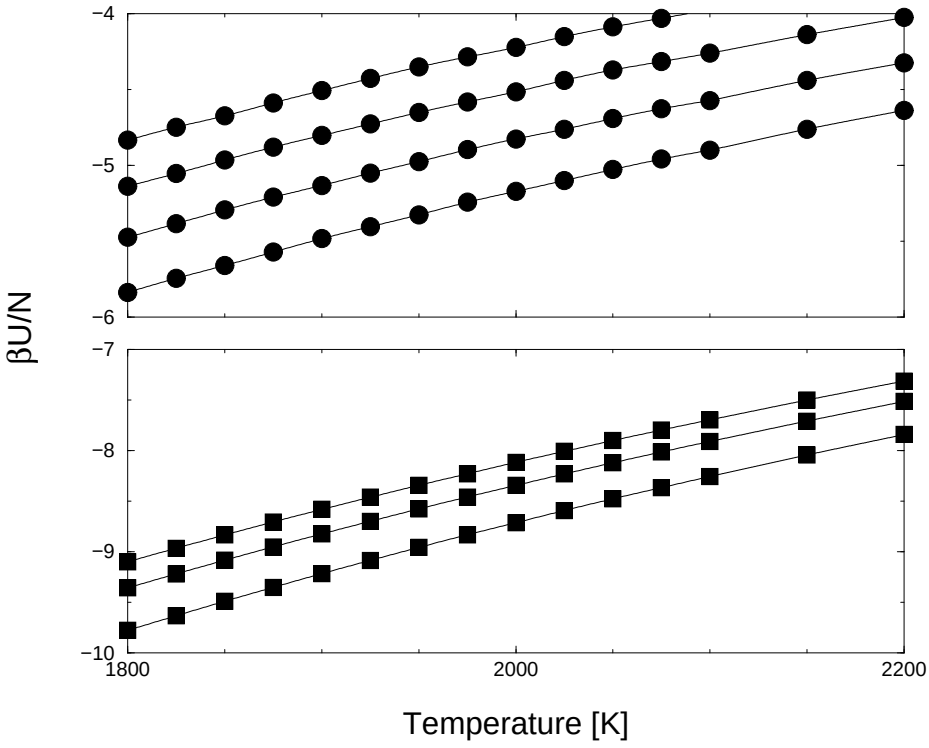


FIG. 4. Internal energy per particle in the fluid (top) and solid (bottom) phases. The behavior along the isochores $\rho = 0.80$, 0.85, 0.90, and 0.95 nm^{-3} (top panel, from top to bottom) and $\rho = 1.251$, 1.27, and 1.305 nm^{-3} (bottom panel, from top to bottom) is shown. Lines are smooth interpolations of the data points.

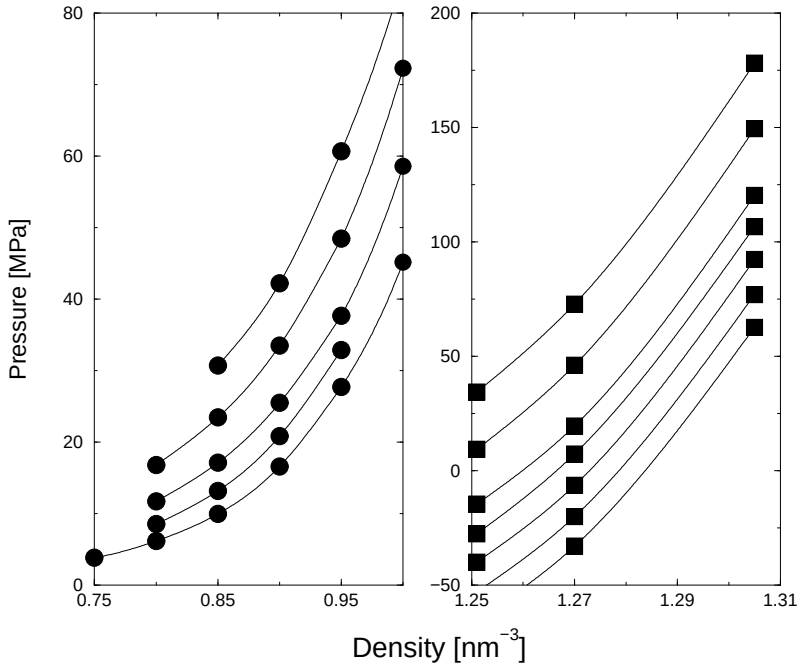


FIG. 5. Equation of state in the fluid (left) and solid (right) phases. The behavior along the isotherms $T = 2200$, 2100, 2000, 1950, and 1900 K (left panel, from top to bottom) and $T = 2200$, 2100, 2000, 1950, 1900, 1850, and 1800 K (right panel, from top to bottom) is shown. Lines are smooth interpolations of the data points.

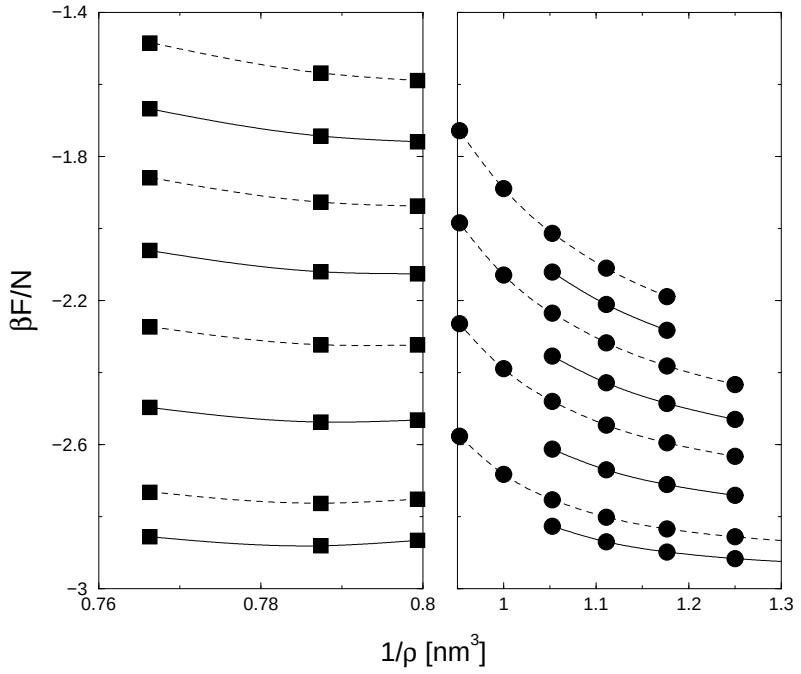


FIG. 6. Helmholtz free energy per particle in the solid (left) and fluid (right) phases. The behavior along the isotherms $T = 2200$, 2150, 2100, 2050, 2000, 1950, 1900, and 1875 K (from top to bottom) is shown. Solid lines are guides to the eye; dashed lines are obtained by integrating Eq. (2), see text.

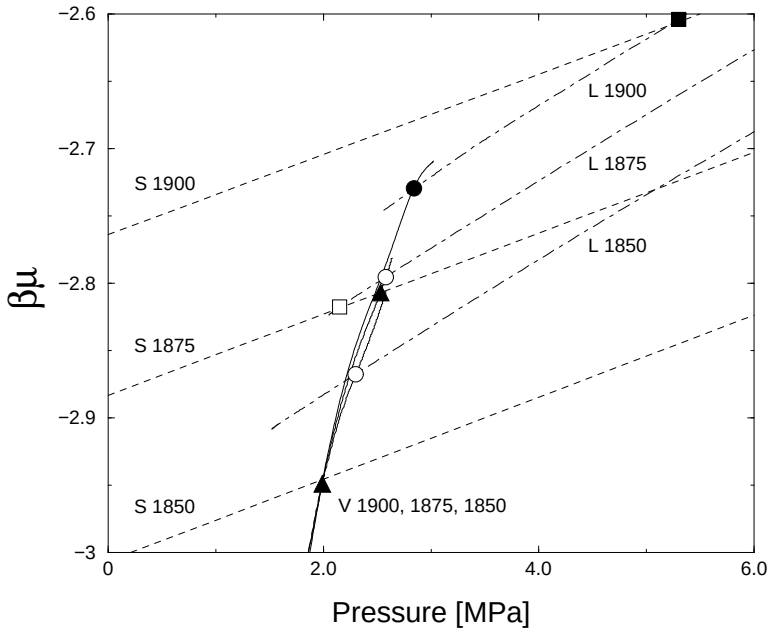


FIG. 7. Chemical potential *vs* pressure in proximity of the triple point, in the vapor (V, full lines), liquid (L, dot-dashed lines) and solid (S, dashed lines) phases at $T = 1900$, 1875, and 1850 K. Liquid-solid (squares), liquid-vapor (circles) and solid-vapor (triangles) coexistence points are shown; full and open symbols refer to stable and metastable equilibria, respectively.

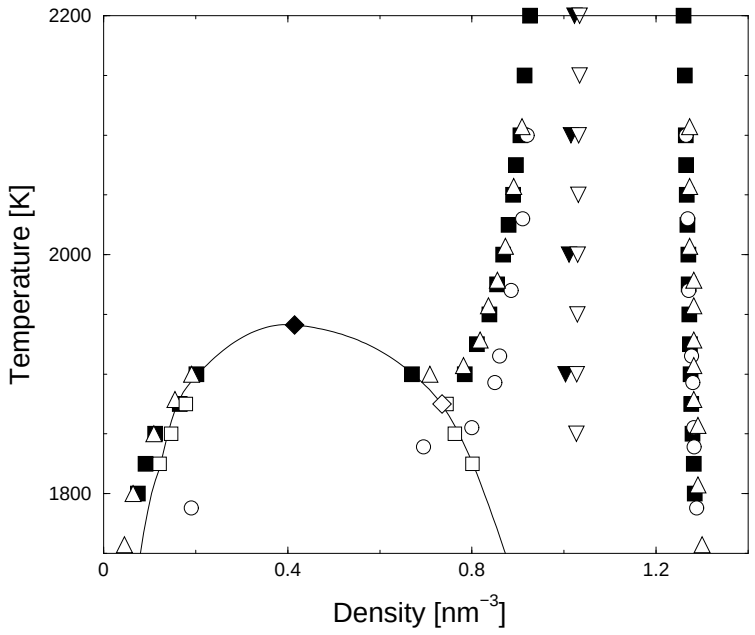


FIG. 8. Phase diagram of the Girifalco model according to the free energy investigation of this work (solid squares, coexistence points; open squares, metastable liquid-vapor separation). The line represents the Gibbs Ensemble Monte Carlo predictions for the liquid-vapor coexistence [15]. The critical (full diamond) and triple (open diamond) points are also shown. Open upward triangles and circles are the simulation results of Ref. [12] and [13], respectively. Open downward triangles: $\Delta s = 0$ *locus*; solid downward triangles: freezing line of the hard-sphere fluid corresponding to the C_{60} model through the WCA prescription (see text).

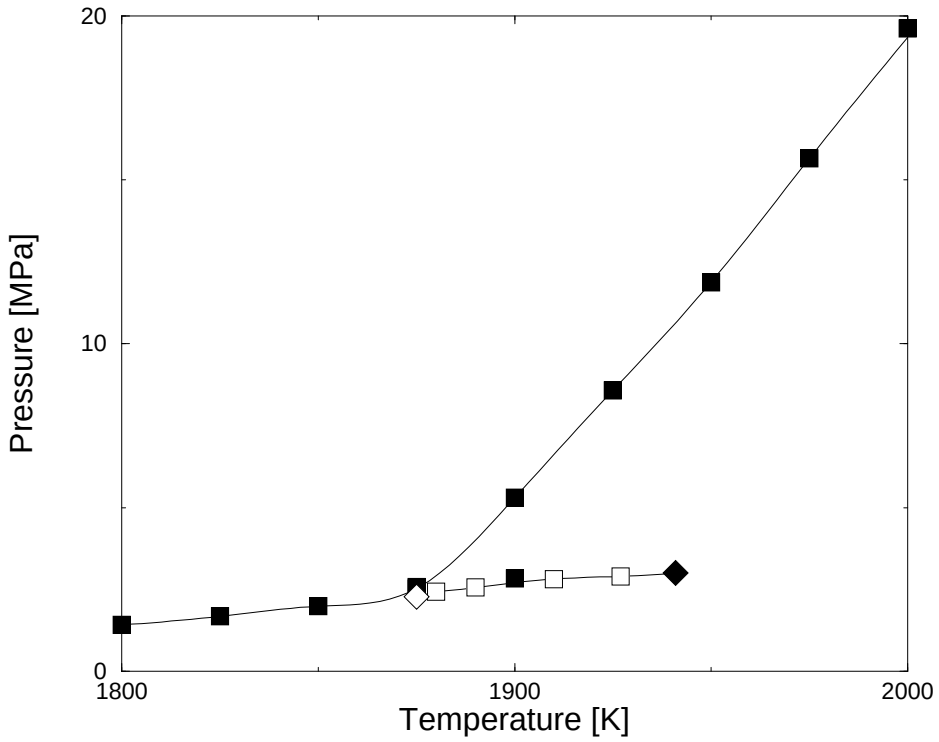


FIG. 9. Phase diagram in the $P - T$ representation. Solid squares, this work; open squares, Gibbs Ensemble liquid-vapor coexistence points [15]. The triple (open diamond) and critical (solid diamond) points are also shown. Lines are intended as guides to the eye.